Article

Soil Gas Measurements of Radon, CO₂ and Hydrocarbon Concentrations as Indicators of Subsurface Hydrocarbon Accumulation and Hydrocarbon Seepage

Marko Cvetković [1,*], Josipa Kapuralić [1], Marija Pejić [1], Iva Kolenković Močilac [1], David Rukavina [1], Duje Smirčić [1], Ana Kamenski [2], Bojan Matoš [1] and Marko Špelić [2]

[1] Faculty of Mining, Geology and Petroleum Engineering, University of Zagreb, Pierottijeva 6, 10000 Zagreb, Croatia; josipa.kapuralic@rgn.unizg.hr (J.K.); marija.pejic@rgn.unizg.hr (M.P.); iva.kolenkovic@rgn.unizg.hr (I.K.M.); david.rukavina@rgn.unizg.hr (D.R.); duje.smircic@rgn.unizg.hr (D.S.); bojan.matos@rgn.unizg.hr (B.M.)
[2] Department of Geology, Croatian Geological Survey, Sachsova 2, 10000 Zagreb, Croatia; akamenski@hgi-cgs.hr (A.K.); mspelic@hgi-cgs.hr (M.Š.)
* Correspondence: marko.cvetkovic@rgn.unizg.hr

Abstract: Soil gas measurements of radon (^{222}Rn), CO₂, and hydrocarbon concentrations, as well as gamma-ray spectrometry, were conducted at two separate locations to estimate the measurement results for known locations of hydrocarbon accumulations in the subsurface and oil seepage on the surface. The aim of the study was to confirm the applicability of the method for identifying migration pathways (e.g., faults) and to detect possible seepages of hydrocarbons to the surface as well as to investigate possible health issue potential about the soil gas analysis results. Site A investigations were performed with a large number of sampling points to provide sufficient spatial coverage to capture the influence of subsurface lithologic variability as well as the influence of the migration pathway on the measured parameters. For the investigation of site B, sampling points were positioned to reflect the situation between the area above producing hydrocarbon fields and areas with no confirmed accumulation. The results presented show that it is possible to distinguish the near-surface lithology (gamma-ray spectrometry), characterize the migration pathway, and indicate the area of oil seepage at the surface. Areas above the known hydrocarbon accumulations generally have elevated radon concentrations and detectable heavier hydrocarbons with sporadic methane in soil gas, which contrasts with the lower radon levels and lack of detectable heavier hydrocarbons in soil gas in the area with no confirmed hydrocarbon accumulation in the subsurface.

Keywords: radon; carbon dioxide; hydrocarbon exploration; soil gas; Croatia

1. Introduction

Soil gas monitoring has numerous exploration applications, including soil contamination by anthropogenic factors [1,2], health risk from radon concentration in urban planning [3,4], earthquake prediction [4,5], and mineral and hydrocarbon resource exploration [6,7]. Monitoring the radon concentration in soil gas is mainly related to radiation risk in residential areas, since radon accounts for more than 50% of radiation dose coming from natural sources [8], probably due to gaseous form of its radioisotopes. Radon has 36 isotopes with atomic masses from 193 to 228 and none of them is stable. In nature, mainly two radioisotopes of radon are present, ^{222}Rn and ^{220}Rn (thoron). ^{222}Rn has half-life 3.8 days, while thoron has half-life of 55.6 s [9]. Radon (^{222}Rn) is produced in uranium bearing rocks and soils by radioactive decay of radium (^{226}Ra), as a part of uranium (^{238}U) decay chain, while thoron is produced from radioactive decay of ^{224}Ra in thorium (^{232}Th) decay chain. Concentration of ^{222}Ra in soil is therefore related to uranium mineralization of soils and concentration of ^{220}Ra is related to thorium concentration in soils.

Non-diffusive transport of radon can be attributed to carrier gas transport [10], so the non-reactive radon represents a suitable tracer for gas transport from the deeper subsurface to the surface. The seepage of methane and other hydrocarbons from hydrocarbon-bearing formations along faults and fractures is well known throughout the world [11,12]. Active faults can be delineated by measuring radon concentrations over the study area; anomalies indicate more emissive zones related either to main faults or secondary fractures [13–15]. The research presented here aims to test the possibility of correlating measured soil gas parameters with hydrocarbon migration pathways in the subsurface (e.g., faults). For this purpose, several soil gas parameters were measured at two different sites (Figure 1). These included the radon (Ra), thoron (^{220}Ra), CO_2, PID (photoionization detector), and TP (total petroleum) concentrations.

Recommended procedures for radon potential maps usually include measurements of radon concentration in soil gas along with soil permeability [16]. Measurements of only these parameters can be difficult to interpret because radon concentrations in soil vary widely, even at short distances, and depend on weather conditions or water content in the soil [17,18]. It is challenging to determine the factors responsible for the variations in radon concentration. Several authors have established a relationship between gamma dose rate and geogenic radon potential [19–22] and have concluded that in situ gamma measurements of U, Th and K can be used to map radon potential. The main advantage of gamma measurements is that they are less time consuming than measurements of radon concentration in soil gas [23]. Gamma ray spectrometry was included for the possible confirmation that potentially elevated radon concentrations were not due to near-surface geological heterogeneity.

Measurements were taken at two sites that were selected based on known locations of hydrocarbon accumulation in the subsurface and oil seepage at the surface. Identification of hydrocarbon migration pathways has wide applicability, not only for petroleum exploration, but also for identifying sources of contamination of groundwater and surface water by hydrocarbons [15]. Hydrocarbons in the environment are persistent and consequently cause disturbance of natural equilibrium between the living species and their natural environment [24,25]. Since they are carcinogens and neurotoxic organic pollutants [26], their presence in the water and soil represents serious threat for human health. While the health threat from ^{222}Rn is mainly limited to residential areas, since soil gas radon which migrates to outdoor air is highly diluted and thus does not present a health risk in open areas, hydrocarbon contamination of soil and water presents a threat even outside of the residential areas.

Presented research indicated possible radon-related health risks in urban planning while the other soil gas parameters and gamma ray spectrometry results were within acceptable boundaries. Radon concentration anomalies, as well as other soil gas parameters were correlated to oil seepage on first exploration location and producing hydrocarbon fields on second location.
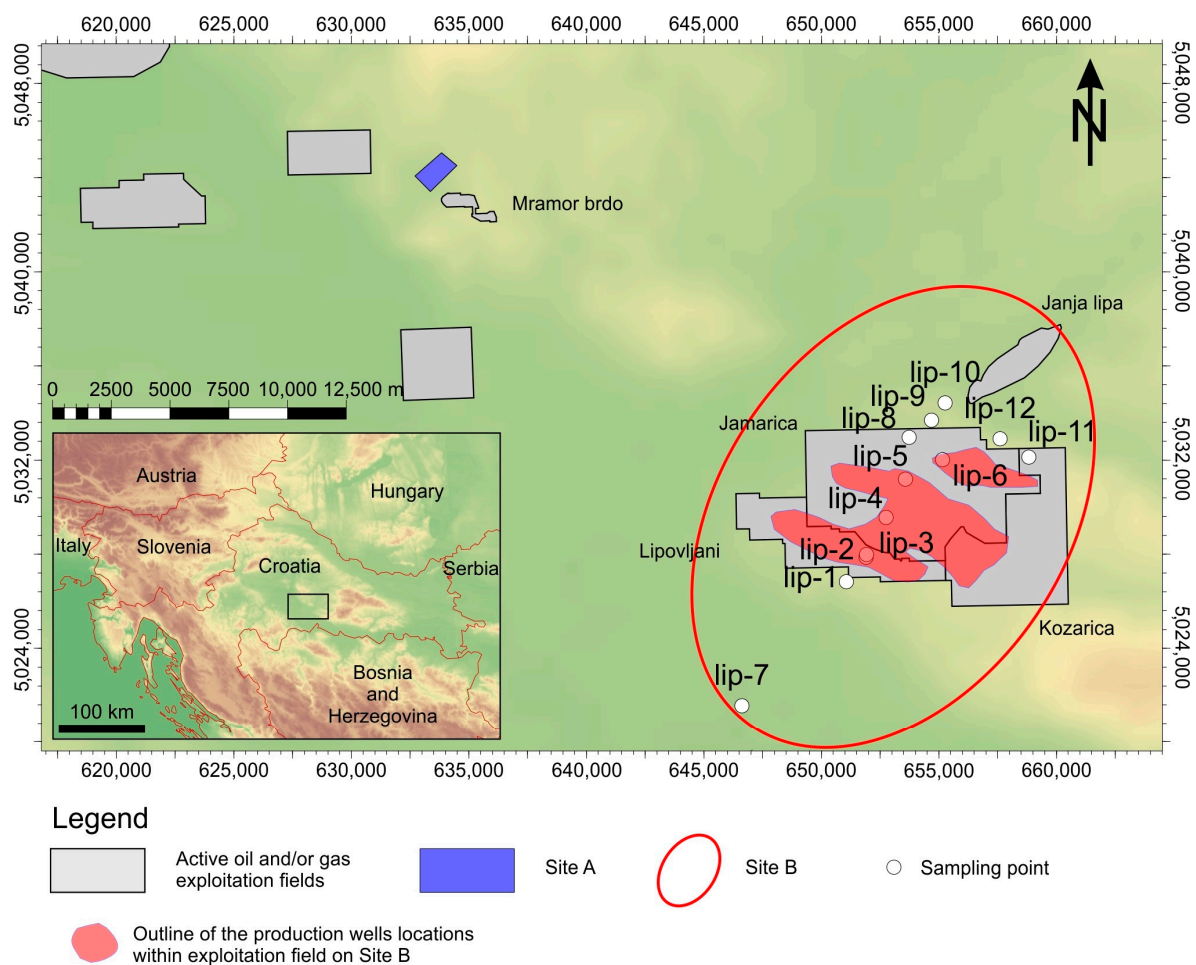
Figure 1. Location map showing the broader area of exploration and locations of Site A and Site B along with oil and/or gas fields. DEM overlay acquired from [27].

2. Materials and Methods

Soil gas measurements were performed at two sites (Figure 1) that were selected due to their known levels of hydrocarbon accumulation in the subsurface and oil seepage at the surface. The measurement points were positioned to cover areas overlying the accumulations and adjacent areas where no accumulations were confirmed. Two areas in the Croatian part of the Pannonian Basin (CPBS) were selected for mapping (Figure 1, Site A) and profiling (Figure 1, Site B). Since the results of soil gas measurements depend not only on the targeted subsurface anomalies (hydrocarbon accumulations, fault zones, and migration pathways) but also on the local geological framework (rock/sediment types), a brief description of the geological setting is necessary to allow subsequent meaningful interpretation of the obtained results.

Site A was selected based on an existing oil seep and historical mining site described in [28] to assess the nature of the migration path of oil to the surface based on soil gas measurements. Site B outlines several areas of hydrocarbon accumulation that were used to test the applicability of soil gas measurements to detect existing accumulation in the subsurface. Measurement points were positioned relative to the locality of the oil seep on Site A, while Site B measurements were positioned to roughly cover both hydrocarbon-producing fields and locations without confirmed hydrocarbon accumulation. The hydrocarbon fields included in the sampling (Figure 1) were Lipovljani (predominantly gas with oil), Jamarice (oil and gas field), and Kozarice (predominantly oil) [29].

2.1. Geological Settings

The research area was situated in the Sava Depression within the Croatian part of Pannonian Basin System (CPBS), which consists of Neogene and Quaternary sediments overlying the Pre-Neogene basement, including Mesozoic and Paleozoic, predominantly metamorphic and magmatic, rocks [30].

The pre-Neogene basement in the vicinity of Site A consists mainly of granite, gneiss, and amphibolite. According to recent studies, the age of these rocks is Cretaceous [31].

Neogene and Quaternary infill can be divided into three megacycles [32,33], representing the relative water level fluctuations in the sedimentation environment [34]. The first megacycle represents the deposition of sediments from the onset of formation of smaller structural units (depressions) within the CPBS, which was not contemporaneous in the system [30,33]. Sedimentation began within the terrestrial environment from the Ottnangian to the Early Badenian, which was followed by marine sedimentation during the Badenian [31,35,36]. Marine sedimentation continued during the Sarmatian, but the connection of Central Paratethys to the surrounding marine environment was terminated, resulting in a decrease in salinity and a transition to brackish environments [37]. Sediments deposited during the first megacycle are characterized by pronounced lithological heterogeneity, ranging from coarse-grained breccias and conglomerates to sandstones, marls, and reef limestones [30,38]. Miocene volcanic rocks are also present in some parts of the CPBS [33,39] but are absent in the study area. The second megacycle of Pannonian age was conditioned by the post-rift regional thermal subsidence processes [40]. The newly formed accommodation space was filled by predominantly turbiditic [30,38] and deltaic [41] sediments in brackish to freshwater Lake Pannon [30,38,41,42]. The sedimentary infill consists mostly of marls, sandstones, and transitional lithologies between these end members. In the Sava Depression and in the research area, this sedimentary succession is considered to be the main hydrocarbon-bearing interval, since the majority of the discovered reservoirs are found in sandstone of Pannonian age [32,43,44]. The third megacycle refers to the last phase of the formation of the CPBS, which involved a transition from lacustrine to terrestrial sedimentary environments of fluvial and marsh types [45,46].

2.2. General Petroleum Geology Settings

CPBS is a known hydrocarbon province with an active petroleum system and more than 70 years of exploration. During this time, more than 100 hydrocarbon fields have been discovered, most of which are still in production [29,47]. Even before conventional hydrocarbon production, heavy oil was produced from mines and refined into lamp oil to be used for district lighting [28]. In the exploration area, the source rocks are represented by Badenian, Sarmatian, and Lower Pannonian marls, while the reservoir rocks are predominantly Pannonian sandstones, although reservoirs can be found in all permeable Neogene sediments, Pliocene, and basement rocks [47]. The sealing rocks are Neogene marls and Pliocene clays. Migration pathways are associated with faults and regional unconformities as well as conveyor beds, through which migration has occurred over distances of up to 60 km, resulting in accumulations near the exploration area [44].

2.3. Radon and Thoron Measurements in Soil Gas

SARAD RTM 2200 is a radon (^{222}Rn) and thoron (^{220}Rn) measurement system that quantifies radon and thoron concentrations and can also measure soil permeability, temperature, humidity, and other technical parameters that indicate proper operation of the instrument. Silicon radiation detectors in the chamber are used to separate the different radon daughter products by alpha spectroscopy. The radon (^{222}Rn) gas concentration is measured by the short-lived daughter products produced by radon decay. The number of ^{218}Po ions collected on a semiconductor detector is proportional to the radon gas concentration in the chamber of the instrument. The half-life of ^{218}Po is 3.05 min, and thus, the equilibrium between the radon decay rate and ^{218}Po detector activity is reached after

about 15 min (about 5 half-lives). This time period is classified as the minimum achievable response time.

The measurements were performed by driving a stainless-steel probe with a detachable tip (outer diameter 12 mm/inner diameter 8 mm) into the soil to a depth of 825 mm. The tip was then hammered a further 125 mm into the ground, providing a filter area for soil gas sampling, which had to be constant as the results of the instrument's permeability measurement were calculated using the specific filter area achieved by this setup. The probe was then connected to the instrument through special tubing which did not allow radon buildup on the material, as that would affect subsequent measurements (Figure 2a). The achievable measurement range was between 0 and 10 MBq/m^3. The device also measured permeability (measuring range from 8×10^{-14} m^2 to 8×10^{-12} m^2) and the CH$_4$ concentration (measuring range from 100 to 25,000 ppm). The soil permeability was determined by measuring the pressure drop in the soil and the air volume flow through the soil. The permeability was calculated within the device itself based on the dimensions of the soil "filter" area made by the impact probe, as shown in Figure 2a.
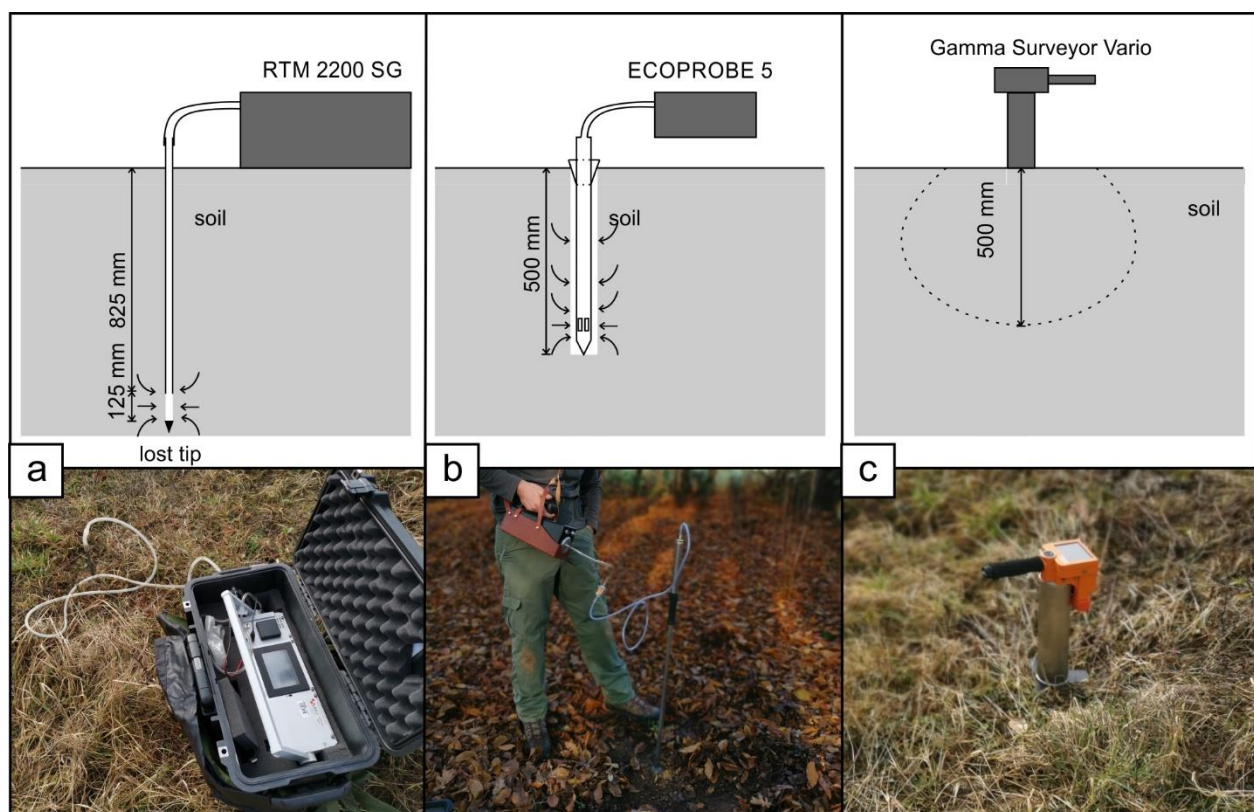

Figure 2. (**a**) Sarad RTM 2200; (**b**) ECOPROBE 5; and (**c**) Gamma Surveyor Vario measuring principles.

2.4. Carbon Dioxide (CO$_2$), Photo-Ionization Analyzer (PID), Total Petroleum (TP), and Methane (CH$_4$) Concentration Measurements in Soil Gas

The measurement of CO$_2$ and CH$_4$ concentrations, volatile organic compounds, and other volatile hydrocarbon components is used to investigate various types of soil contamination, such as hydrocarbon contamination, and also to monitor in situ bioremediation processes, which are mostly aerobic, meaning that bacteria break down hydrocarbons by oxidation to produce heat, methane, and carbon dioxide.

CO$_2$ has been proven to be the carrier gas for radon in faulted clay basins overlying sedimentary rocks such as limestones, marls, and sandstones, in cases where all sediments have a low uranium content [48]. The measurement of the CO$_2$ concentration along with the TP and methane concentrations could help to distinguish higher concentrations originating

from hydrocarbon seepage and migration in the subsurface from local background levels. Methane is also considered to be a gas carrier for radon [49].

These components were measured using the ECOPROBE 5 monitor, which measures the concentration of a contaminant vapor phase in a subsurface soil environment. It consists of two independent analyzers: a photo-ionization detector (PID, measures the total concentration of volatile organic compounds), and an infrared analyzer (IR, separately measures methane, the petroleum group of hydrocarbons (TP), and carbon dioxide. It also measures the temperature, atmospheric pressure, and oxygen concentration.

Measurement started by drilling a hole about 50 cm deep in the ground with a hand drill, inserting a probe into the hole, and closing it quickly with the sealing cone (Figure 2b). Due to the nature of the measurement, a waiting period between inserting the probe into the soil and starting the measurement is recommended, and this waiting period must be consistent for all sampling points. In this study, the standby time was 60 s. During sampling, lower permeability soil has a tendency for CO_2 buildup to occur with a high depletion rate (values after the start of the test decrease rapidly). Thus, in later representation of these values, averaged values of CO_2 and PID are also presented to minimize the influences of these gases in poorly permeable soils.

The sensitivity of the PID analyzer in standard mode ranges from 0.1 to 2000 ppm. The IR analyzer has a lower detection limit of 50 ppm, and the measurement range goes up to 500,000 ppm for methane and TP.

2.5. Natural Gamma-Ray Spectrometry

The Gamma Surveyor Vario with the VB6 BGO probe is a geophysical gamma-ray spectrometer that is used for the determination of the concentrations of K [%], U [ppm] and Th [ppm] as well as the natural gamma dose rate [nGy/h or nSv/h]. The detector is a Bismuth Germanium Oxide (BGO) scintillator. Measurement errors for determination of the K, U, and Th concentrations and the natural gamma dose rate are mainly influenced by the measurement time used. However, there is no generally recommended measurement time. The sampling time required for a measurement depends on the radioactivity of the source and the desired measurement accuracy. The final measurement errors depend on the absolute values of the individual K, U, and Th concentrations or their mutual combinations. For a detector placed on the ground, the effective depth of investigation is about 50 cm (variable depending on the type of sample), and a similar radius with a soil/rock mass of more than 100 kg affects the measurement (Figure 2c). In our measurements, the detector was placed on the ground, and the measurement time was 5 min.

Radon emanates from materials containing the unstable radionuclides ^{232}Th and ^{238}U. In particular, the ^{238}U decay series forms gaseous ^{222}Rn via alpha decay of solid radium (^{226}Ra) [50,51].

The decay of ^{238}U and its daughters in soil and rock forms radon. The amount of ^{238}U contained in the soil and underlying rock of an area directly affects the amount of geogenic ^{222}Rn released in that area. Observation of gamma emission rates along with bedrock and surface geology can improve the interpretation of radon readings. Gamma measurements were performed in order to relate gamma values to the radon concentration in soil gas, which is helpful for interpreting radon readings. We wanted to investigate whether there was a correlation between near-surface gamma values and radon concentrations that would indicate that measured radon concentrations result only from local geologic changes.

It is known that radiation values decrease above petroleum accumulations. This phenomenon has been attributed to either [52,53] the precipitation of uranium salts at the oxidation–reduction boundary between the aqueous phase and hydrocarbon accumulation or [54] the conversion of K-bearing clay minerals and feldspars to kaolinite or other potassium-deficient clays.

3. Results

3.1. Site A

A total of 55 sampling points were obtained at Site A (Figure 3). All measurements have ECOPROBE 5 and gamma-ray spectrometry data, while additional radon and thoron levels were measured at 18 points. The lower radon and thoron values resulted from the fact that measurements could not be taken at some locations because the high level of soil moisture resulted in low permeability, which fell below the instrument threshold, and because those were more time consuming due to the nature of the measurement. Sampling points were more densely distributed near the areas of oil seepage in the river and at the oil mine. To identify the possible migration pathway, an outline of the faults is given based on the published maps (Geological map of the area [55]).
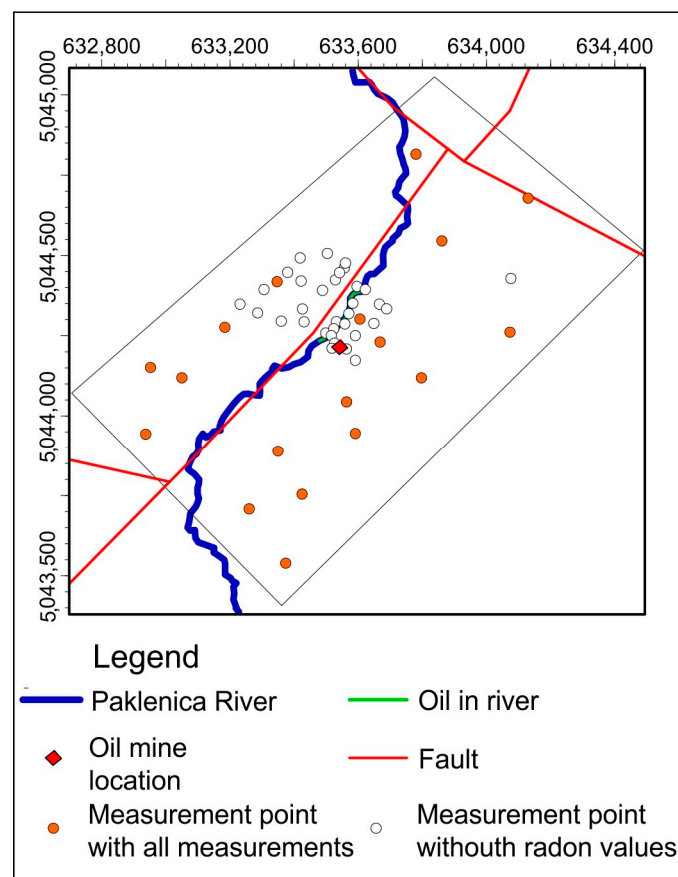

Figure 3. Measurement locations on Site A, locations of the faults were obtained from [55].

Measurement results of all three methods were mapped within the Site A area with Schlumberger Petrel. The gamma-ray spectrometry results indicated variations in soil composition that are directly related to the underlying bedrock. The fault with an SSW–NNE orientation represents a boundary between the bedrock that is predominantly marl west of the fault and the mixed marl-sandstone lithology east of the fault. The dose rate (DR) was increased in the western area (Figure 4d) in correspondence to the clay content in the marls. Elevated values of potassium (K, Figure 4a) and thorium (Th, Figure 4c) were also predominantly found in the western area, while the uranium content was variable within the exploration area (U, Figure 4b). Lower values of U, Th, and DR were registered in the SE area of Site A where sandstone outcrops were observed. Locally, lower values of all three elements and DR were observed around the oil seepage and oil mine.
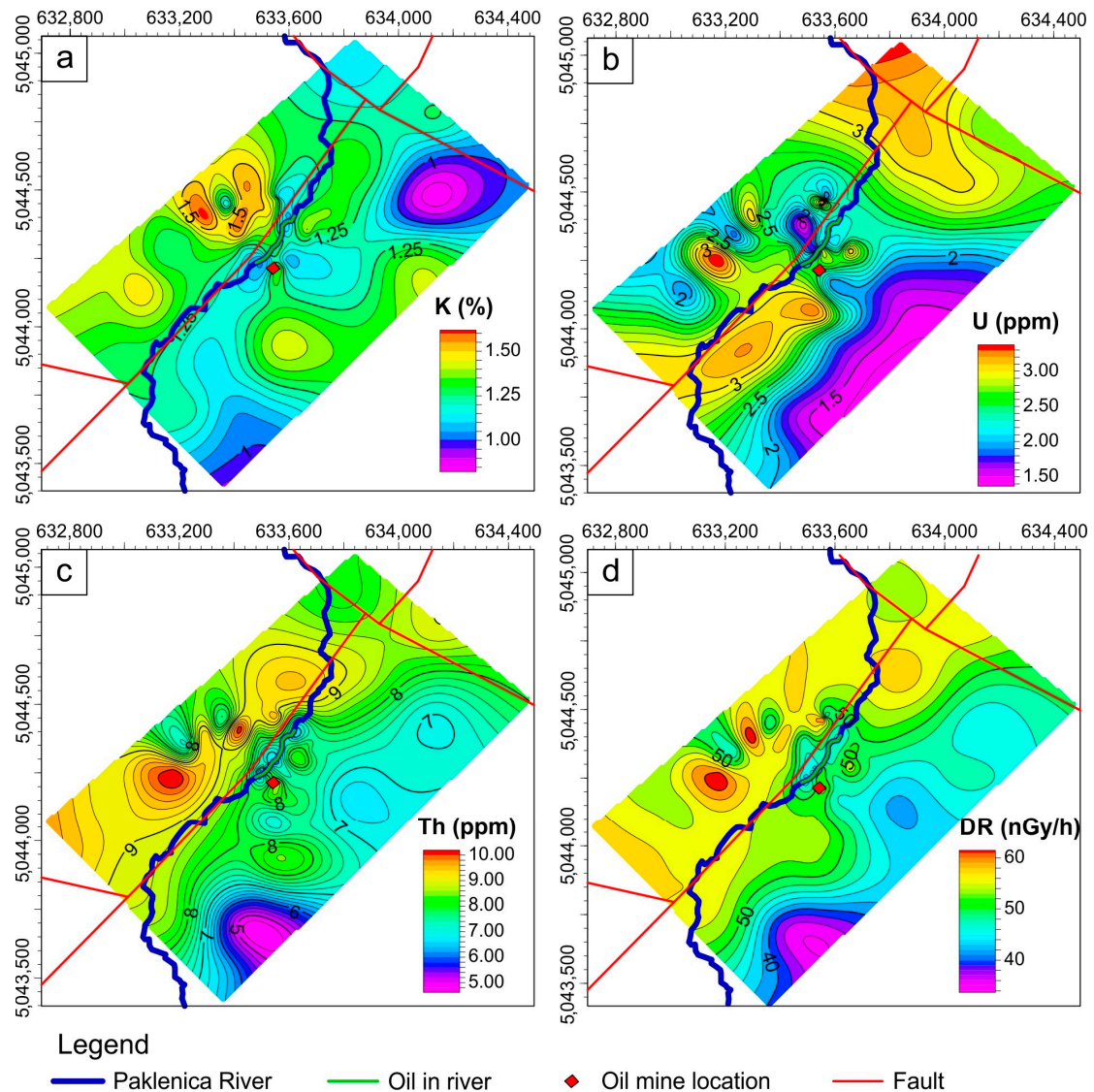
Figure 4. Spatial distribution of: (**a**) potassium (K); (**b**) uranium (U); and (**c**) thorium (Th) and (**d**) the total dose rate (DR).

ECOPROBE 5 measurements are presented using the following parameters: maximum recorded concentration of CO_2 (CO_2_max), average concentration of CO_2 (CO_2_avg), maximum recorded concentration of volatile organic compounds (PID_max), average concentration of volatile organic compounds (PID_avg), and maximum concentration of volatile hydrocarbons (TP). The average and maximum values were obtained during 60 s of soil gas sampling. Increases in both PID_max (Figure 5a) and PID_avg (Figure 5b) values were identified east of the fault and east of the oil seepage and oil mine. The CO_2_max values (Figure 5c) were variable throughout Site B, while the CO_2_avg values (Figure 5d) showed an increase in the area surrounding the oil seepage. TP values were only recorded near the seepage (Figure 5e).
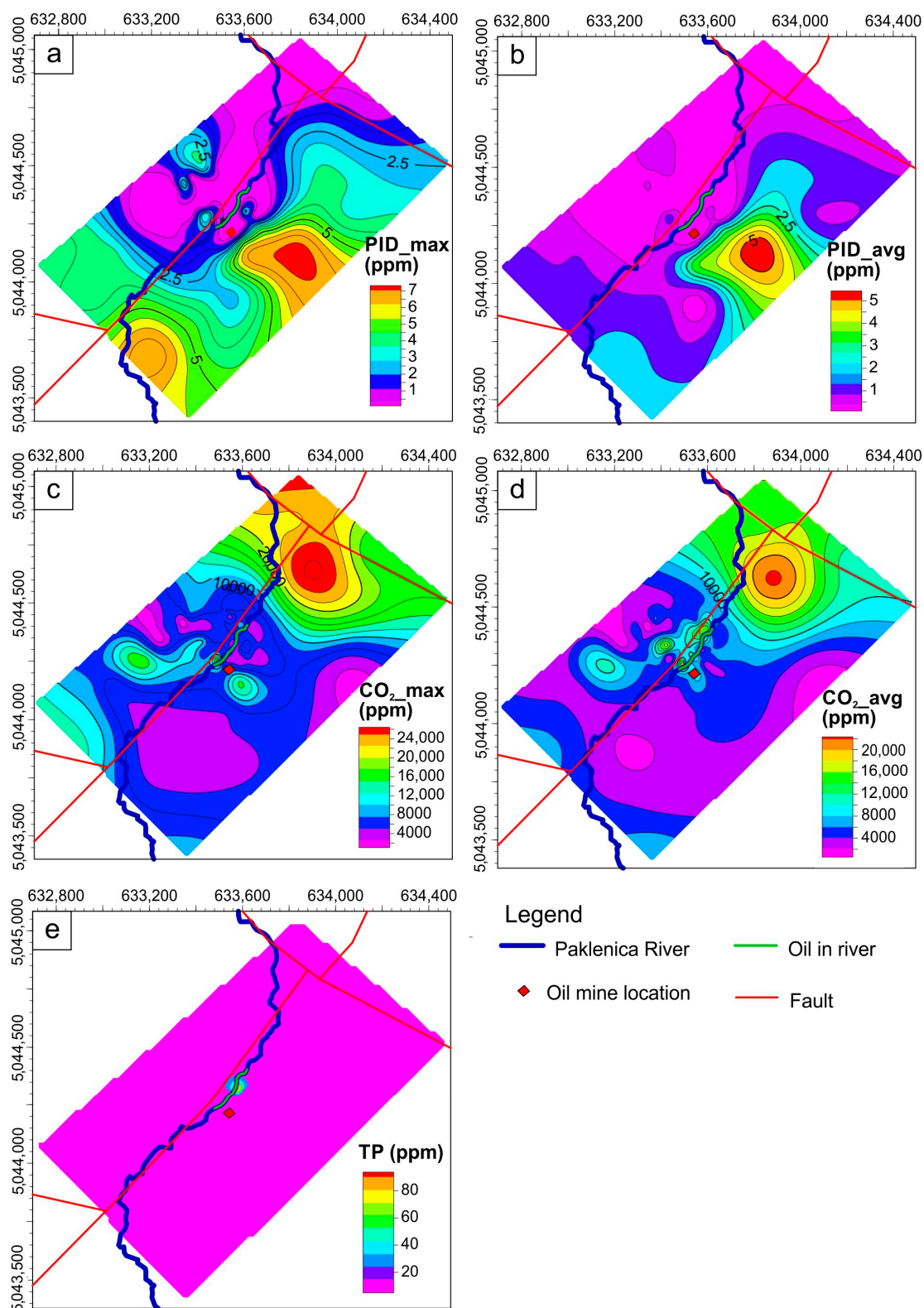
Figure 5. Photo-ionization analyzer (PID) (**a**,**b**); CO_2 (**c**,**d**); and Total Petroleum (TP) (**e**) concentrations recorded at Site A.

Elevated radon concentrations were recorded in the area near the fault (Figure 6a), but were generally very variable within Site A. This was also seen for the thoron levels (Figure 6b). The distribution of the radon/thoron ratio showed a clear anomaly in the area near the oil seepage (Figure 6c). The recorded permeability values were variable within Site A (Figure 6d) and negative correlated with the radon values, which is in accordance

with the normal occurrence of radon values in impermeable soils [56]. Distinct anomalies were recorded for the radon (Figure 6a), permeability (Figure 6d), CO_2_max, and CO_2_avg maps NE of the oil seepage. Radon risk potential map (Figure 6e) was constructed based on measured radon concentrations in soil gas and soil permeability according to [56,57]. Majority of the area is characterized as high and medium risk potential.
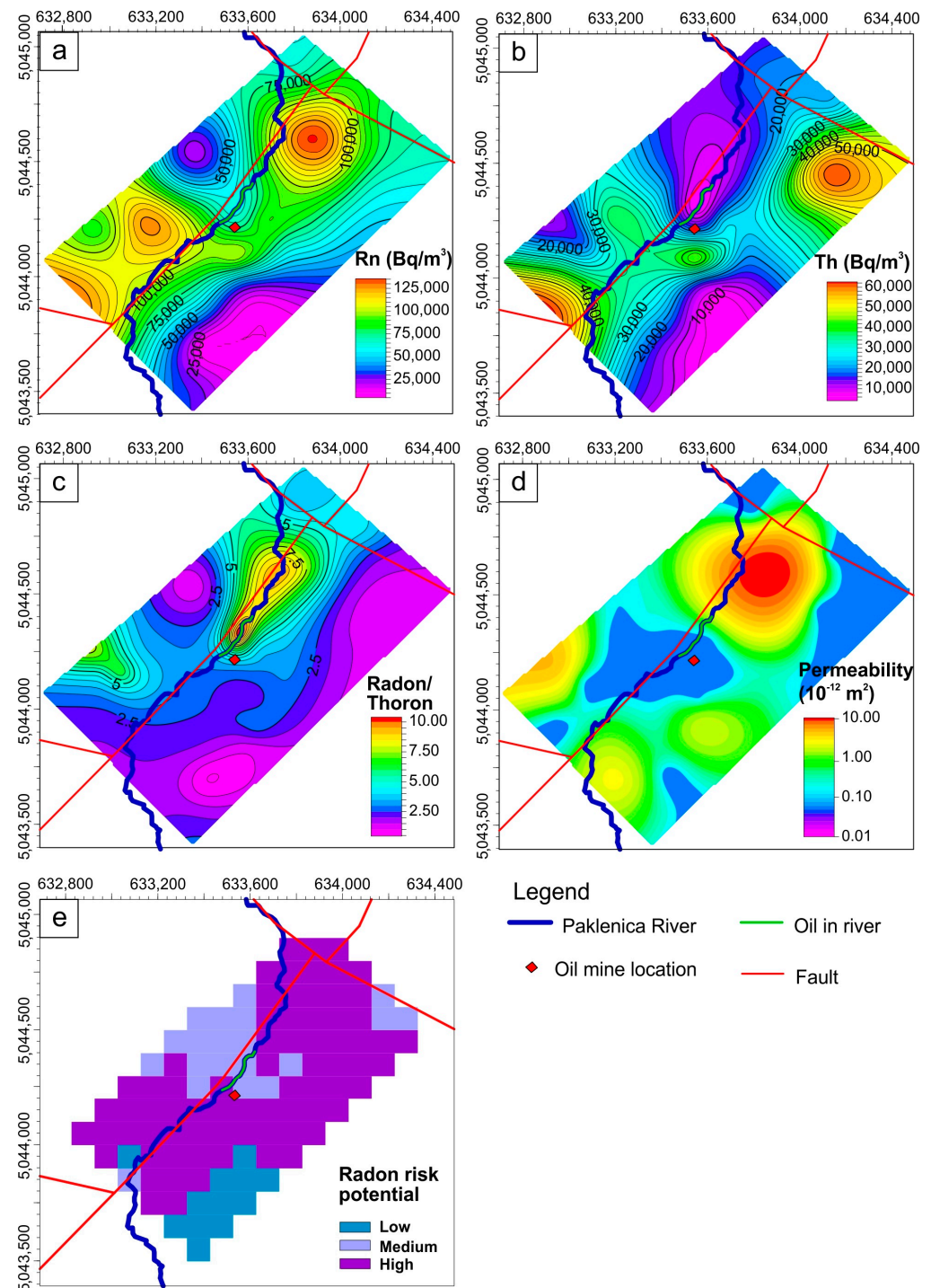

Figure 6. Radon (**a**); thoron (**b**); radon/thoron ratio (**c**); and permeability distribution (**d**) within Site A. Radon risk potential is presented on (**e**) according to [56,57].

To test the relation of the CO_2 and radon concentrations in soil gas Pearson correlation coefficient was calculated [58]. Dataset for this case was divided into two groups containing

measurements from either NW or SE of the fault (Figure 7). Pearson correlation coefficient show moderate positive relation but with *p* value greater than 0.05 for the data belonging to the area NW of the fault. Analysis from the SE side of the fault shows a strong positive correlation while the *p* value in this case is lower than 0.05.
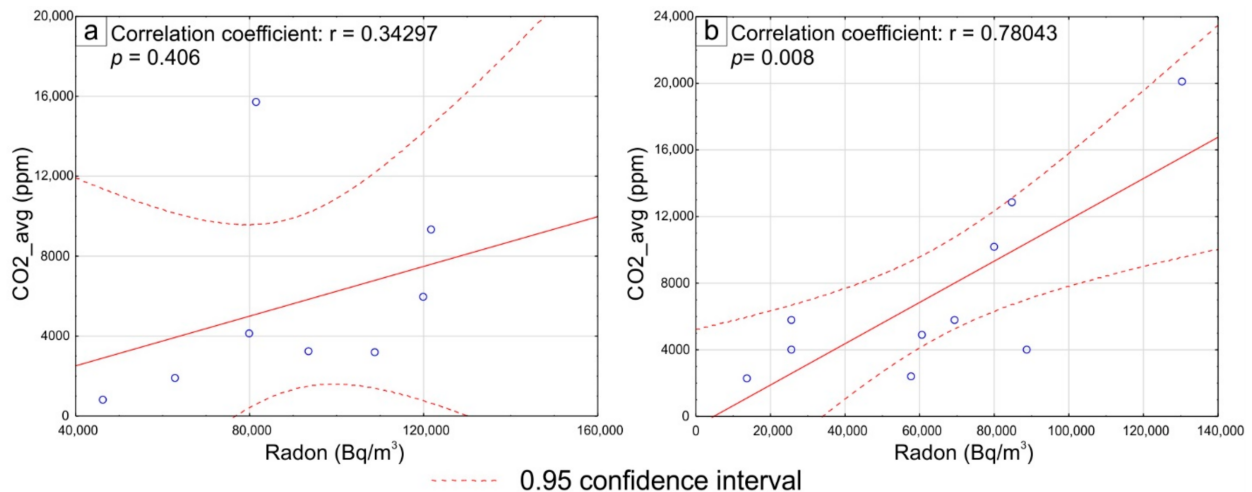

Figure 7. Scatterplots showing relation to radon/CO_2 relation on the West (**a**) and E side (**b**) of the fault parallel to the river.

3.2. Site B

Site B was selected to test the applicability of using soil gas measurements to detect hydrocarbon seepage from underlying accumulation areas. Some of the sampling points selected were located above known production fields, while others were positioned in areas with no evidence of existing accumulation. Twelve sampling points were obtained, five of which were located over known production fields (Figure 1). The sampling points included radon and thoron measurements along with CO_2, PID, TP, and CH_4 concentrations in the soil gas. The results are presented in Tables 1 and 2. Uncertainty for radon and thoron measurements were presented for 95% confidence interval based on the sensitivity of the RTM 2200 SG (3 counts per minute/(kBq/m^3)) and achieved counts over a 15-min period.

Table 1. The measured concentrations of radon and thoron in the soil gas at 12 sampling points on Site B (locations shown in Figure 1). Bolded values refer to location within hydrocarbon-producing fields.

Sample ID	Radon (Bq/m^3)	Thoron (Bq/m^3)
lip-1	56,465 (+/− 2195)	24,277 (+/− 1439)
lip-2	**102,174 (+/− 2953)**	**22,482 (+/− 1385)**
lip-3	**86,665 (+/− 2720)**	**24,456 (+/− 1444)**
lip-4	**112,763 (+/− 3102)**	**27,940 (+/− 1544)**
lip-5	**105,254 (+/− 2997**	**28,137 (+/− 1549)**
lip-6	**119,781 (+/− 3197)**	**20,180 (+/− 1312)**
lip-7	79,621 (+/− 2607)	17,125 (+/− 1209)
lip-8	94,390 (+/− 2838)	32,217 (+/− 1658)
lip-9	73,533 (+/− 2505)	16,695 (+/− 1193)
lip-10	81,936 (+/− 2644)	34,026 (+/− 1704)
lip-11	107,165 (+/− 3024)	19,362 (+/− 1285)
lip-12	82,325 (+/− 2651)	34,521 (+/− 1716)

Table 2. The measured concentrations of radon, thoron, maximum CO_2, average CO_2, maximum PID, average PID, Total Petroleum, and methane in the soil gas at 12 sampling points on Site B (locations shown in Figure 1). Bolded values refer to location within hydrocarbon-producing fields. "-" corresponds to a concentration below the measuring limit.

Sample ID	CO_2_max (ppm)	CO_2_avg (ppm)	PID_max (ppm)	PID_avg (ppm)	TP (ppm)	CH_4 (ppm)
lip-1	4280	2629	4.69	1.82	-	-
lip-2	**4720**	**3064**	**44.81**	**28.02**	**135**	-
lip-3	**4063**	**3414**	**4.36**	**1.94**	**99.3**	-
lip-4	**4676**	**3903**	**1.93**	**0.97**	**430**	-
lip-5	**5519**	**3634**	**3.14**	**1.48**	**551.7**	-
lip-6	**18,892**	**9574**	**1.24**	**0.16**	**2439**	**1846**
lip-7	16,251	11,486	-	-	-	-
lip-8	3145	1834	1.46	0.13	-	-
lip-9	3325	2217	2.93	0.84	-	-
lip-10	6115	5892	2.83	2.34	-	-
lip-11	7022	4154	2.98	0.64	-	-
lip-12	6819	4724	1.98	0.83	-	-

TP values were recorded only within the area delineating active production fields, while a CH_4 concentration above 50 ppm was only recorded at one location, which was also within the boundaries of the oil producing field. Radon concentrations were generally elevated in the area of hydrocarbon producing fields (Table 2). TP values increased from the predominantly gas-bearing field (Lipovljani, Figure 1, lip-2 and 3), to the mixed oil and gas field Jamarica (lip-4 and 5), to the predominantly oil-bearing field Kozarice (Figure 1, lip-6).

4. Discussion

The anomalies of PID and TP at Site A along the Paklenica River can be associated with the existing seepage along the SW–NE oriented fault, where the values of these parameters are elevated in the soil in the area characterized by lower permeability, indicating a localized concentration of migrated hydrocarbons along the fault as well as a lower oxidative biodegradation intensity. The correlation between permeability and increased CO_2 concentration can be explained by the increased oxygen supply in permeable soil at a depth of 50 cm, where it is expected that intense biodegradation by oxidation will result in the depletion of organic compounds and, consequently, an increase in the CO_2 concentration. Moreover, according to [59], the CO_2 concentration in soil depends on the soil texture. Many authors have emphasized the influences of temperature and humidity on the CO_2 concentration in soil gas [60,61]. Obviously, a higher water content promotes the ability of soil to keep CO_2 in the dissolved state. The fact that the measurements were performed during the cold and wet season (late autumn and winter) suggests that higher CO_2 concentrations could be expected during the dry season. Difference between the Pearson correlation coefficient in the CO_2 and radon concentrations in soil gas from the NW and SE side of the fault suggest the possibility of CO_2 acting as a carrier gas from the deeper parts of the subsurface as stated in [48].

Changes in surface radiometric measurements have relatively small magnitudes and should be distinguished by statistical analysis of a larger number of measurements. However, the relative relationships observed in the presented data are discussed here. The radon concentration was characterized by spatial variability, reflecting the heterogeneity of the soil/rock environment unless it is transported from deeper subsurface by a carrier gas [62,63]. This is evident to the NE of the fault, where radon concentrations show a positive correlation to CO_2 concentrations in soil gas which implies a possible transport or radon by a carrier gas. It should also be considered that soil permeability affects fluid and gas migration in the rock and has a significant effect on radon measurements. The maximum radon concentrations presented may indicate that gases are transported from greater depths in areas near faults, but relatively elevated radon concentrations (SW and

NE part of Site A) could also be associated with elevated concentrations of Uranium. In the area with oil leakage, the concentration of Th was relatively stable with respect to the concentrations of U and K. Upwelling hydrocarbons can alter the radiometric signatures above oil fields as they saturate the rocks, and this leads to reduced sorption of the mobile radionuclides U and K in the overlying rocks [64]. Carbonic acid in groundwater produced by the decomposition of hydrocarbons can also leach potassium and uranium from the soil. The concentration of uranium depends on a dynamic equilibrium between the rate of leaching and the amount of enrichment, while the potassium concentration always decreases due to leaching [53,65], a phenomenon that could also explain the lower concentration of potassium in the area surrounding the oil seep. Since ^{222}Rn has a longer half-life ($T_{1/2}$ = 3.82 d) than thoron ($T_{1/2}$ = 55.6 s), the radon/thoron ratio can indicate whether gases are transported from greater depths through a fault system or they have a local origin. In our measurements, the radon/thoron ratio showed a clear anomaly along the N part of the Paklenica River and the SSW–NNE fault, especially in the area of the oil leakage. TP values were only recorded at some points near the oil seepage, possible as a result of oil at the seepage site being heavily biodegraded [66]. Majority of radon index values [57] calculated for Site A belong to high and medium radon risk category which requires further research directed to possible health issues and indoor radon measurements in the study area. Gamma ray spectrometry revealed that the total DR rarely exceeds average population weighted world-averaged of 60 nGy/h [8] while the mean value for the area is 50.4 nGy/h.

The samples from Site B show distinct TP anomalies in the area of the hydrocarbon-producing field, demonstrating that leakage from the oil and gas fields in the subsurface through clastic sediments can be identified. This was further proven by the increase in the radon concentration as well as the methane and CO_2 concentrations at the lip-6 sampling point. PID values were detected in all sampling points above or near hydrocarbon accumulations with the exception of lip-7, which is far from oil and/or gas fields.

5. Conclusions

The results presented show correlations of radon, thoron, CO_2, and hydrocarbon concentrations in soil gas with the occurrence of oil seepage on the surface and proven hydrocarbon accumulation in the subsurface. This has not been investigated previously in the CPBS. Radon/thoron ratios at Site A indicate a migration pathway from the deeper subsurface through elevated concentrations of the longer half-life ^{222}Rn (radon) relative to the shorter half-life ^{220}Rn (thoron) in soil gas. Gamma-ray spectrometry values presented at Site A can be used to distinguish changes in the shallow subsurface lithology and can also indicate alterations in rock and soil mineralogy due to the presence of hydrocarbons.

Measured parameters are characterized by emphasized spatial variability, in part reflecting the heterogeneity of the mineralogical characteristics of the near-surface rocks, so results from larger number of sampling points should be compared with detailed data on soil/rock properties in order to obtain more reliable interpretation. Currently available data on surface geological settings do not allow such comparisons. Medium to high risk of radon radiation indicated for the Site A requires further research directed to possible health issues and indoor radon measurements in the study area.

Author Contributions: Conceptualization, M.C. and I.K.M.; methodology, M.C., J.K., I.K.M. and M.P.; software, M.C., D.R. and A.K.; validation, I.K.M. and M.C.; formal analysis, M.C., I.K.M. and A.K.; investigation, J.K., M.P., I.K.M., D.S., D.R.; writing—original draft preparation, M.C., J.K., M.P., A.K., I.K.M. and M.Š.; writing—review and editing, B.M., M.Š.; visualization, M.C. and B.M.; supervision, M.C.; project administration, M.C.; funding acquisition, M.C. and I.K.M. All authors have read and agreed to the published version of the manuscript.

References

1. Chylkova, J.; Machalikova, J.; Obrsalova, I.; Brunclik, T.; Bata, R. Monitoring of Methane and CO_2 from Selected Sources in the Environment in the Czech Republic. In Proceedings of the Recent Advances in Environment, Ecosystems and Development, Canary Islands, Spain, 14–16 December 2009; pp. 96–103.
2. Hendel, J. Occurrence of Microbial and Thermogenic Gases in Post-Mining Areas. In Proceedings of the 17th International Multidisciplinary Scientific GeoConference SGEM2017, Energy and Clean Technologies, Albena, Bulgaria, 29 June–5 July 2017.
3. Cinelli, G.; Tositti, L.; Capaccioni, B.; Brattich, E.; Mostacci, D. Soil gas radon assessment and development of a radon risk map in Bolsena, Central Italy. *Environ. Geochem. Health* **2015**, *37*, 305–319. [CrossRef]
4. Tokonami, S. Characteristics of Thoron (^{220}Rn) and Its Progeny in the Indoor Environment. *Int. J. Environ. Res. Public Health* **2020**, *17*, 8769. [CrossRef] [PubMed]
5. Sugisaki, R.; Ido, M.; Takeda, H.; Isobe, Y.; Hayashi, Y.; Nakamura, N.; Satake, H.; Mizutani, Y. Origin of Hydrogen and Carbon Dioxide in Fault Gases and Its Relation to Fault Activity. *J. Geol.* **1983**, *91*, 239–258. [CrossRef]
6. Partington, J.R. Discovery of Radon. *Nat. Cell Biol.* **1957**, *179*, 912. [CrossRef]
7. Füst, A.; Geiger, J. Monitoring planning and evaluation using geostatistics, I.Geostatistical support for verification sampling based on professional opinion. *Földtani Közlöny* **2010**, *140*, 303–312.
8. UNSCEAR. *Sources and Effects of Ionizing Radiation, Volume I: Sources*; United Nations: New York, NY, USA, 2000.
9. Jönsson, G. Radon gas—Where from and what to do? *Radiat. Meas.* **1995**, *25*, 537–546. [CrossRef]
10. Kristiansson, K.; Malmqvist, L. Evidence for nondiffusive transport of 86Rn in the ground and a new physical model for the transport. *Geophysics* **1982**, *47*, 1444–1452. [CrossRef]
11. Khilyuk, L.F.; Chilingar, G.V.; Robertson, J.O.; Endres, B. Surface Soil-Gas Surveys. In *Gas Migration*; Elsevier BV: Amsterdam, The Netherlands, 2000.
12. Dyck, W.; Jonasson, I. Chapter 11 Radon. In *Drainage Geochemistry*; Elsevier BV: Amsterdam, The Netherlands, 2000; Volume 7, pp. 353–394.
13. Aubert, M.; Baubron, J.-C. Identification of a hidden thermal fissure in a volcanic terrain using a combination of hydrothermal convection indicators and soil-atmosphere analysis. *J. Volcanol. Geotherm. Res.* **1988**, *35*, 217–225. [CrossRef]
14. Neri, M.; Giammanco, S.; Leonardi, A. Preliminary Indoor Radon Measurements Near Faults Crossing Urban Areas of Mt. Etna Volcano (Italy). *Front. Public Health* **2019**, *7*, 7. [CrossRef]
15. Palacios, D.; Fusella, E.; Avila, Y.; Salas, J.; Teixeira, D.; Fernandez, G.; Salas, A.; Sajo-Bohus, L.; Greaves, E.; Barros, H.; et al. Radon measurements over a natural-gas contaminated aquifer. *Radiat. Meas.* **2013**, *50*, 116–120. [CrossRef]
16. Szabó, K.Z.; Jordan, G.; Horváth, Á.; Szabó, C. Mapping the geogenic radon potential: Methodology and spatial analysis for central Hungary. *J. Environ. Radioact.* **2014**, *129*, 107–120. [CrossRef] [PubMed]
17. Thu, H.N.P.; Van Thang, N.; Hao, L.C. The effects of some soil characteristics on radon emanation and diffusion. *J. Environ. Radioact.* **2020**, *216*, 106189. [CrossRef]
18. Yang, J.; Busen, H.; Scherb, H.; Hürkamp, K.; Guo, Q.; Tschiersch, J. Modeling of radon exhalation from soil influenced by environmental parameters. *Sci. Total. Environ.* **2019**, *656*, 1304–1311. [CrossRef] [PubMed]
19. Fernández, C.S.; Poncela, L.Q.; Villar, A.F.; Merino, I.F.; Gutierrez-Villanueva, J.; González, S.C.; López, L.Q.; Fernández, E.; Tejerina, J.R.; Matarranz, J.M.; et al. Spanish experience on the design of radon surveys based on the use of geogenic information. *J. Environ. Radioact.* **2017**, *166*, 390–397. [CrossRef] [PubMed]
20. Melintescu, A.; Chambers, S.; Crawford, J.; Williams, A.; Zorila, B.; Galeriu, D. Radon-222 related influence on ambient gamma dose. *J. Environ. Radioact.* **2018**, *189*, 67–78. [CrossRef]
21. Cinelli, G.; Tollefsen, T.; Bossew, P.; Gruber, V.; Bogucarskis, K.; De Felice, L.; De Cort, M. Digital version of the European Atlas of natural radiation. *J. Environ. Radioact.* **2019**, *196*, 240–252. [CrossRef]
22. García-Talavera, M.; García-Pérez, A.; Rey, C.; Ramos, L. Mapping radon-prone areas using γ-radiation dose rate and geological information Related content Mapping radon-prone areas using γ-radiation dose rate and geological information. *J. Radiol. Prot.* **2013**, *33*, 605–620. [CrossRef]
23. Tchorz-Trzeciakiewicz, D.; Rysiukiewicz, M. Ambient gamma dose rate as an indicator of geogenic radon potential. *Sci. Total. Environ.* **2021**, *755*, 142771. [CrossRef]
24. Hentati, O.; Lachhab, R.; Ayadi, M.; Ksibi, M. Toxicity assessment for petroleum-contaminated soil using terrestrial invertebrates and plant bioassays. *Environ. Monit. Assess.* **2012**, *185*, 2989–2998. [CrossRef]

25.   Péter, O.; Abioye, O.P. Biological Remediation of Hydrocarbon and Heavy Metals Contaminated Soil. In *Soil Contamination*;
        IntechOpen: London, UK, 2011.

26.   Das, N.; Chandran, P. Microbial Degradation of Petroleum Hydrocarbon Contaminants: An Overview. *Biotechnol. Res. Int.* **2011**,
        2011, 1–13. [CrossRef]

27.   Eea Eudem—Copernicus Land Monitoring Service. Available online: https://land.copernicus.eu/homepage-content/eu_dem.
        png/view (accessed on 10 August 2020).

28.   Gretić, Z.; Bobić, D. *From Oil Outcrops to Oil Fields [Od Paklina do Naftnih Polja]*; INA d.d.: Zagreb, Croatia, 2002.

29.   Velić, J.; Krasić, D.; Kovačević, I. Exploitation, reserves and transport of natural gas in the Republic of Croatia. *Tech. Vjesn. Gaz.*
        2012, *13*, 633–641.

30.   Pavelić, D.; Kovačić, M. Sedimentology and stratigraphy of the Neogene rift-type North Croatian Basin (Pannonian Basin System,
        Croatia): A review. *Mar. Pet. Geol.* **2018**, *91*, 455–469. [CrossRef]

31.   Balen, D.; Petrinec, Z. Contrasting tourmaline types from peraluminous granites: A case study from Moslavačka Gora (Croatia).
        Miner. Pet. **2011**, *102*, 117–134. [CrossRef]

32.   Saftić, B.; Velić, J.; Sztanó, O.; Juhász, G.; Ivković, Ž. Tertiary subsurface facies, source rocks and hydrocarbon reservoirs in the SW
        part of the Pannonian Basin (Northern Croatia and south-western Hungary). *Geol. Croat.* **2003**, *56*, 101–122.

33.   Lučić, D.; Saftić, B.; Krizmanić, K.; Prelogović, E.; Britvić, V.; Mesić, I.; Tadej, J. The Neogene evolution and hydrocarbon potential
        of the Pannonian Basin in Croatia. *Mar. Pet. Geol.* **2001**, *18*, 133–147. [CrossRef]

34.   MIitchum, R.M.J. Seismic Stratigraphy and Global Changes of Sea Level, Part 11: Glossary of Terms used in Seismic Stratigraphy.
        In *Seismic Stratigraphy–Applications to Hydrocarbon Exploration*; Payton, U., Ed.; AAPG: Tulsa, OK, USA, 1977; pp. 205–212.

35.   Ćorić, S.; Pavelić, D.; Rögl, F.; Mandić, O.; Vrabac, S.; Avanić, R.; Jerković, L.; Vranjković, A. Revised Middle Miocene datum
        for initial marine flooding of North Croatian Basins (Pannonian Basin System, Central Paratethys). *Geol. Croat.* **2009**, *62*, 31–43.
        [CrossRef]

36.   Kováč, M.; Andreyeva-Grigorovich, A.; Bajraktarević, Z.; Brzobohatý, R.; Filipescu, S.; Fodor, L.; Harzhauser, M.; Nagymarosy,
        A.; Oszczypko, N.; Pavelić, D.; et al. Badenian evolution of the Central Paratethys Sea: Paleogeography, climate and eustatic
        sea-level changes. *Geol. Carpathica* **2007**, *58*, 579–606.

37.   Piller, W.E.; Harzhauser, M.; Mandic, O. Miocene Central Paratethys stratigraphy—Current status and future directions. *Stratigra-
        phy* **2007**, *4*, 151–168.

38.   Pavelic, D. Cyclicity in the evolution of the neogene north Croatian basin (Pannonian Basin System). In *Developments in
        Sedimentology*; Elsevier BV: Amsterdam, The Netherlands, 2005; pp. 273–283.

39.   Malvić, T.; Cvetković, M. Lithostratigraphic units in the Drava Depression (Croatian and Hungarian parts)—A correlation. *Nafta*
        2013, *63*, 27–33.

40.   Horváth, F.; Bada, G.; Szafián, P.; Tari, G.; Ádám, A.; Cloetingh, S. Formation and deformation of the Pannonian Basin: Constraints
        from observational data. *Geol. Soc. Lond. Mem.* **2006**, *32*, 191–206. [CrossRef]

41.   Sebe, K.; Kovačić, M.; Magyar, I.; Krizmanić, K.; Špelić, M.; Bigunac, D.; Sütő-Szentai, M.; Kovács, Á.; Szuromi-Korecz, A.; Bakrač,
        K.; et al. Correlation of upper Miocene–Pliocene Lake Pannon deposits across the Drava Basin, Croatia and Hungary. *Geol. Croat.*
        2020, *73*, 177–195. [CrossRef]

42.   Geary, D.; Magyar, I.; Muller, P. Ancient Lake Pannon and its endemic molluscan fauna (Central Europe; mio-pliocene). *Adv. Ecol.
        Res.* **2000**, *31*, 463–482. [CrossRef]

43.   Velic, J.; Malvic, T.; Cvetkovic, M.; Vrbanac, B. Characteristics of hydrocarbon fields in the Croation part of the Pannonian basin.
        Oil Gas Eur. Mag. **2010**, *36*, 146–147.

44.   Velić, J. *Geologija Nafte [Petroleum Geology]*; University of Zagreb, Faculty of Mining, Geology and Petroleum Engineering: Zagreb,
        Croatia, 2007.

45.   Brkić, Ž. The relationship of the geological framework to the Quaternary aquifer system in the Sava River valley (Croatia). *Geol.
        Croat.* **2017**, *70*, 201–213. [CrossRef]

46.   Cvetković, M. Possibilities for Well Log Correlation using Standard Deviation Trends in Neogene-Quaternary Sediments, Sava
        Depression, Pannonian Basin. *Geol. Croat.* **2017**, *70*, 79–85. [CrossRef]

47.   Velić, J.; Malvić, T.; Cvetković, M.; Vrbanac, B. Reservoir geology, hydrocarbon reserves and production in the Croatian part of
        the pannonian Basin System. *Geol. Croat.* **2012**, *65*, 91–101. [CrossRef]

48.   Etiope, G.; Lombardi, S. Evidence for radon transport by carrier gas through faulted clays in Italy. *J. Radioanal. Nucl. Chem.* **1995**,
        193, 291–300. [CrossRef]

49.   Durrance, E.M.; Gregory, R.G. Helium and radon transport mechanisms in hydrothermal circulation systems of Southwest
        England. In *Geochemistry of Gaseous Elements and Compounds*; Theophrastus Pub. S.A.: Athens, Greece, 1990; pp. 337–352.

50.   Hanrahan, G. *Key Concepts in Environmental Chemistry*; Elsevier BV: Amsterdam, The Netherlands, 2012.

51.   Schwela, D.; Kotzias, D. Pollution, Air Indoor. In *Encyclopedia of Toxicology*; Elsevier: Amsterdam, The Netherlands, 2005;
        pp. 475–489.

52.   Latyshova, M.G.; D'Yakonova, T.F. Reliability evaluation for geological and geophysical information in calculating oil and gas
        reserves. *Int. Geol. Rev.* **1981**, *23*, 977–982. [CrossRef]

53. Schumacher, D. Hydrocarbon-Induced Alteration of Soils and Sediments. In *Hydrocarbon Migration and Its Near-Surface Expression*; Schumacher, D., Abrams, M.A., Eds.; American Association of Petroleum Geologists: Vancouver, BC, Canada, 1996; pp. 71–89. ISBN 9781629810812.

54. Heemstra, R.; Ray, R.; Wesson, T.; Abrams, J.; Moore, G. *Critical Laboratory and Field Evaluation of Selected Surface Prospecting Techniques for Locating Oil and Natural Gas*; Department of Energy, Artlesville Energy Technology Centre: Bartlesville, OK, USA, 1979.

55. Crnko, J. *Geological Map of Croatia–Kutina*; Croatian Geological Survey: Zagreb, Croatia, 2014.

56. Neznal, M. Permeability as an important parameter for radon risk classification of foundation soils. *Ann. Geophys.* **2005**, *48*, 175–180.

57. Barnet, I.; Pacherova, P.; Neznal, M. *Radon in Geological Environment-Czech Experience*; Czech Geological Survey: Prague, Czech Republic, 2008; ISBN 978-80-7075-707-9.

58. Barbur, V.A.; Montgomery, D.C.; Peck, E.A. Introduction to Linear Regression Analysis. *J. R. Stat. Soc. Ser. D* **1994**, *43*, 339. [CrossRef]

59. Kiefer, R.H.; Amey, M.R.G. Concentrations and controls of soil carbon dioxide in sandy soil in the North Carolina coastal plain. *Catena* **1992**, *19*, 539–559. [CrossRef]

60. Enoch, H.; Dasberg, S. The occurrence of high CO_2, concentrations in soil air. *Geoderma* **1971**, *6*, 17–21. [CrossRef]

61. Gregory, R.; Durrance, E. Helium, carbon dioxide and oxygen soil gases: Small-scale variations over fractured ground. *J. Geochem. Explor.* **1985**, *24*, 29–49. [CrossRef]

62. Wilkening, M. Radon transport processes below the Earth's surface. In *The Natural Radiation Environment, III*; US Department of Energy: Washington, DC, USA, 1980; pp. 90–104.

63. Ilie, A.M.C.; Vaccaro, C. Atmospheric and Soil Methane Concentrations Integrating a New Gas Detection Technology. In Proceedings of the 1st International Electronic Conference on Applied Sciences, Tokyo, Japan, 10–30 November 2020.

64. Matolín, M.; Stráník, Z. Radioactivity of sedimentary rocks over the Ždánice hydrocarbon field. *Geophys. J. Int.* **2006**, *167*, 1491–1500. [CrossRef]

65. Fernández, D.P.; Fusella, E.; Avila, Y.; Salas, J.; Teixeira, D.; Fernández, G.; Sajo-Bohus, L.; Greaves, E.; Barros, H.; Bolívar, M.; et al. Soil gas radon and thoron measurements in some Venezuelan oilfields. *J. Radioanal. Nucl. Chem.* **2015**, *307*, 801–810. [CrossRef]

66. Kovačević, M. Petrological, Petrophysical and Geochemical Features of the Miocene Deposits of Požega Valley. Master's Thesis, University of Zagreb, Zagreb, Croatia, 2017.